GEODETIC MONITORING OF BRIDGE DEFORMATIONS OCCURRING DURING STATIC LOAD TESTING

Tarvo Mill[1]✉, Artu Ellmann[2], Martti Kiisa[3], Juhan Idnurm[4], Siim Idnurm[5], Milan Horemuz[6], Andrus Aavik[7]

[1, 2, 4, 5, 7]*Dept of Road Engineering, Tallinn University of Technology, Ehitajate tee 5, 19086 Tallinn, Estonia*
[3]*Faculty of Construction, Tallinn University of Applied Sciences, Pärnu mnt 62, 10135 Tallinn, Estonia*
[6]*Dept of Geodesy and Geoinformatics, Royal Institute of Technology, Drottning Kristinas väg 30,*
10044 Stockholm, Sweden
E-mails: [1]tarvo@tktk.ee; [2]artu.ellmann@ttu.ee; [3]martti.kiisa@tktk.ee; [4]juhan.idnurm@ttu.ee;
[5]siim.idnurm@ttu.ee; [6]milan.horemuz@abe.kth.se; [7]andrus.aavik@ttu.ee

Abstract. Terrestrial laser scanning technology has developed rapidly in recent years and has been used in various applications but mainly in the surveying of different buildings and historical monuments. The use for terrestrial laser scanning data for deformation monitoring has earlier been tested although conventional surveying technologies are still more preferred. Since terrestrial laser scanners are capable of acquiring a large amount of highly detailed geometrical data from a surface it is of interest to study the metrological advantages of the terrestrial laser scanning technology for deformation monitoring of structures. The main intention of this study is to test the applicability of terrestrial laser scanning technology for determining range and spatial distribution of deformations during bridge load tests. The study presents results of deformation monitoring proceeded during a unique bridge load test. A special monitoring methodology was developed and applied at a static load test of a reinforced concrete cantilever bridge built in 1953. Static loads with the max force of up to 1961 kN (200 t) were applied onto an area of 12 m² in the central part of one of the main beams; the collapse of the bridge was expected due to such an extreme load. Although the study identified occurrence of many cracks in the main beams and significant vertical deformations, both deflection (–4.2 cm) and rising (+2.5 cm), the bridge did not collapse. The terrestrial laser scanning monitoring results were verified by high-precision levelling. The study results confirmed that the TLS accuracy can reach ±2.8 mm at 95% confidence level.

Keywords: Terrestrial Laser Scanning, precise levelling, load testing, monitoring deformations, cantilever beam.

1. Introduction

In recent years Terrestrial Laser Scanning (TLS) has became more widely used in surveying of different structures. The main advantage of using TLS technology in such projects lies in its capability of acquiring a complete set of data of the whole surface of interest within a short period of time. TLS also enables surveying of inaccessible parts of structures with a high level of detail. Advantageously the technology does not rely on specific reference points as are needed for conventional technologies such as levelling and tacheometry. A thorough overview of the TLS technology can be found in Staiger (2003), Quintero *et al.* (2008), Reshetyuk (2009) and Vosselman and Maas (2009). The quality analysis of TLS can be found in Reshetyuk (2010) and Lichti (2010).

Geodetic deformation monitoring of different structures is conducted commonly by using either total station observations, precise levelling, terrestrial photogrammetry or GPS (Global Positioning System) surveys. Fairly seldom TLS has been used in deformation monitoring due to the novelty of the technology. Nevertheless, deformation monitoring using TLS technology is reported by Tsakiri and Pfeifer (2006), who gave an assesement of the quality of results and also reviewed aspects that are recommended to be considered for such research. Monserrat and Crosetto (2008) applied the least squares 3D surface matching (a method proposed originally by Gruen and Akca (2005)) to identify deformations based on repeated TLS scans. Riveiroa *et al.* (2013) validates TLS technology and photogrammetric techniques for deformation monitoring, the resulting TLS accuracy was estimated to reach 10 mm.

The main purpose of conducting a load test of an existing bridge is to acquire information on the carrying capacity of the structure, which condition has been influenced by

age and traffic. The need for load testing arises from doubts about the quality of construction or design or when some visible damage has occurred. The load testing is particularly valuable where public confidence is involved. Also a load test may be intended to establish the behaviour of a structure, analysis of which might otherwise be impossible for a variety of reasons (Bungey, Millard 1996). During bridge load tests elements of the beams are streched allowing the beam to bend. Thus there is a need to determinine deformations of inaccessible parts of the structure of the bridge, such as the bottom surface of the beams.

This study focuses on geodetic monitoring of bridge deformations occurring during static load test. Two surveying technologies: TLS and precise levelling were used for this. A similar work is reported by Zogg and Ingensand (2008) who described deformation monitoring at a load test of a viaduct using a TLS and precise levelling simultaneously at the deck of a viaduct itself. The main objective of the present study is to explore the behaviour of the bridge structures during the load test with extreme static loads – according to the pre-calculations the bridge was expected to collapse. This prevented placing the TLS monitoring station either on or under the bridge deck. An accuracy assessment of using TLS technology in unfavourable and hazardous survey conditions is investigated. Precise levelling results are used for verifying TLS data accuracy. A brief summary concludes the paper.

2. Bridge load tests

Bridge load tests provide researchers and bridge engineers with valuable information about the actual behaviour of structure. There are always some discrepancies between precalculations and the actual test results, since different calculation methods involve several variables and usually adopt some simplifications. Sometimes the structure is too damaged for adequate evaluations of the load-bearing capacity.

Bridges are tested either using static or dynamic loads. For static load tests (depending also on expected outcome) heavy vehicles (dumper trucks, army tanks, etc.) or heavy items (metal blocks, sand bags, etc.) are usually placed on bridge deck. Displacements, deformations and the incipiency of cracks in the structure are investigated during the test, Fig. 1.

Static load tests can be divided into three groups: appending, proving and destructive load test (Ryall 2001).
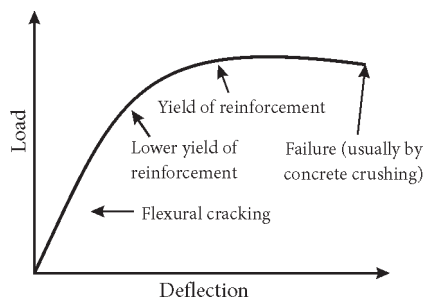

Fig. 1. Typical load deflection curve for under-reinforced beam (Bungey, Millard 1996)

The appending load test is the most common testing method, and it is usually carried out by bringing a load to bearing support that is up to 70% of the designed load value without causing any permanent damage to the structure. The actual test results are usually compared with pre-calculated values to determine whether the selected calculation method was correct or not. The results also show the technical condition of the structure. In proving load tests the load is selected to be equal to the load that is theoretically destructive to particular bridge. This method provides direct proof of the actual carrying capacity of the bridge, but there is a significant risk of damage to the bridge structure. The third option is to load the bridge up to the point of destruction. This load test is rarely used – mostly on old bridges which will be demolished during or after the testing anyways, the main aim being to provide information on the current physical condition of similar type bridges elsewhere. The destructive method was used in this case study.

Dynamic load testing provides data on the dynamic behaviour of the structure such as displacements, deformations, natural frequencies, mode shapes and damping. Dynamic load tests are considered more hazardous, due to the vibrations caused in the structure, as they generally lead to extensive damage. In the case of dynamic load tests, a vehicle with several axles and a specific weight travelling on the bridge at various speeds is generally used. For short bridges the dynamic load test is rarely carried out.

There are many procedures to be carried out before and after the bridge load test. Just before the test, a detailed inspection of the structure must be conducted. It is vital to record the initial state of the structure, since after the load testing it would not be possible. Pre-calculations are needed for estimating expected magnitude of deformations occurring during the load test. Theoretical pre-calculations describe the behaviour of the structure during the test and evaluate the critical moment and mode of the structure's failure. There are usually two types of pre-calculations – one based on the original design (technical documentation, drawings etc) and the other, on the actual parameters (e.g. in situ measured dimensions, material properties). Prior the test, a test plan is usually formulated where all actions involved in the testing are described in detail. The testing ends with a thorough final report which contains, in addition to the analysis of the test results, a description of the procedures carried out before and after the test.

Load testing of bridges is not required by law in Estonia, but in practice there is a need for about 2–5 tests every year. *Estonian Road Administration* acknowledges that even though several international standards related to load testing (*ISO 2394:1998 General Principles on Reliability for Structures, ISO 13822:2010 Bases for Design of Structures – Assessment of Existing Structures, ISO 14963:2003 Mechanical Vibration and Shock – Guidelines for Dynamic Tests and Investigations on Bridges and Viaducts, ISO 18649:2004 Mechanical Vibration – Evaluation of Measurement Results from Dynamic Tests and Investigations on Bridges* etc.)

exist, but there is a need for developing comprehensive national guidelines for this complicated procedure. The present case study is meant to be a step towards development of bridge load testing guidelines for Estonia.

There are around 950 state highway bridges in Estonia, 82% of which are made from reinforced concrete, 69% of which have a total length of 3–25 m, and 64% of which were built between 1950 and 1990. The structures of these bridges were mostly standardised, e.g. the case study bridge had a structure typical of the 1950-ies. The *Estonian Road Administration* is interested in investigating these bridges more thoroughly, since heavy vehicles, salting of the roads, complicated climate conditions (the amount of rainfall exceeding evaporation and temperatures fluctuating substantially around 0 °C, resulting in the corrosion of reinforcement steel bars and the cracking of concrete), inappropriate technical solutions, and insufficient maintenance over the decades have degraded the load carrying capacity of these bridges.

3. Review on geodetic monitoring technologies

In overall, there are different devices that are used to determine characteristics of deformations such as strain gauges, inclinometers, crack microscopes, rulers and callipers. Geodetic instruments include precise levelling instruments, total stations, terrestrial laser scanners and terrestrial photogrammetric instruments.

However no static devices were used in the case study due the risk of structural failure thus the possibility of shattering the assembled devises. Since the case study used two geodetic monitoring techniques – precise levelling and TLS, their principles are briefly reviewed below.

3.1. Precise levelling

Precise levelling measurement is considered the most accurate way of determining heights and is expected to provide the best quality of results in deformation monitoring process. Precise levelling uses highly accurate levelling instruments and levelling staff(s). The data processing is simple and very straightforward. The observing procedures applied in precise levelling are more rigorous than in general engineering levelling. Sub-millimetre accuracy is only achieved by using modern levelling instruments in conjunction with calibrated invar levelling staff(s).

3.2. Terrestrial laser scanning

Based on scanning technology, TLS's are divided into triangulation, Time of Flight (TOF) and Phase-Shift (PS) scanners.

Triangulation laser scanners are mainly used in applications generally requiring an operating range that is less than 25 m; nonetheless triangulation scanners have very high accuracies in the order of tenth of millimetres. In principle triangulation scanners are considered also as terrestrial laser scanners, but due to the limited working range, they may not be categorized in the same group of terrestrial laser scanners (Schulz 2007).

TOF laser scanners make use of short laser pulses by which they scan their entire field of view one point at a time by changing the range finder's direction. The view direction of the laser range finder is changed by a deflection unit (Quintero *et al.* 2008). Since the laser pulse travels with a constant speed, the speed of light, the distance between the scanner and the object is determined with the following expression (Vosselman, Maas 2009):

$$\rho_i = \frac{ct}{2r}, \tag{1}$$

where ρ_i – the range of the ith point with respect to scanner location; c – the speed of light in vacuum (i.e. 299 792 458 m/s).

If the light waves travel in the air-filled environment then a correction factor equal to the refractive index, which depends on the air temperature, pressure and humidity, must be applied to c, e.g. according to Vosselman and Maas (2009) $r \approx 1.00025$. Typical pulsed TOF laser scanners measure up to 50 000 points per second. The distance accuracy of TOF scanners depends mostly on timing accuracy resulting normally an accuracy of 4 to 10 mm.

In PS laser scanners the emitted (incoherent) light is modulated in amplitude and fired onto a surface. The scattered reflection is collected and a circuit device measures the phase difference between the sent and received wave-forms, hence a time delay. According to the distance measuring equation of the TOF scanners, the distance to the target can be found by the demodulation of the back-scattered signal by means of four sampling points that are triggered to the emitted wave (Quintero *et al.* 2008):

$$\rho_i = \frac{c\Delta\Phi}{4\pi f_{mod}}, \tag{2}$$

where $\Delta\Phi$ – phase difference; f_{mod} – modulation frequency.

This method allows faster measuring, up to 1 000 000 points per second, typically within ranges under 100 m. The accuracy of PS scanners depends on the modulated wavelength and the signal to noise (SNR) ratio resulting normally in an accuracy of 2 to 5 mm (Quintero *et al.* 2008).

Thus, a TLS is able to acquire a large number of points within seconds; the acquired data forms a point cloud:

$$\left\{ \left(x_i, y_i, z_i, I(x_i, y_i, z_i) \right), \ i = 1, \ \ldots, \ n \right\}, \tag{3}$$

where x_i, y_i, z_i denote the coordinates of the ith survey point in the scanner's intrinsic coordinate system; $I(x_i, y_i, z_i)$ – the intensity related to the ith point; n – the number of acquired survey points. Intensity is a value of the returned signal strength, which is usually stored as a unitless number in the range of 0 to 2^8. If the scanner is equipped with a digital photo camera, the colour values from the photos are also added to each survey point. The coordinates (x_i, y_i, z_i) of the ith survey point with respect to the scanner's intrinsic coordinates are determined using the point's

spherical polar coordinates: range, horizontal direction, and vertical angle.

In order to transform the coordinates from the intrinsic coordinate system to some extrinsic coordinate system (e.g. national) a rigid-body transformation is used (cf. also Mill *et al.* 2014).

$$\begin{bmatrix} x_i^E \\ y_i^E \\ z_i^E \end{bmatrix} = \begin{bmatrix} x_S^E \\ y_S^E \\ z_S^E \end{bmatrix} + \mathbf{R}_3(\kappa)\mathbf{R}_2(\varphi)\mathbf{R}_1(\omega) \begin{bmatrix} x_i \\ y_i \\ z_i \end{bmatrix}, \qquad (4)$$

where $\left(x_i^E, y_i^E, z_i^E\right)$, $i = 1, \ldots, n$ denote the coordinates of a scanned point i in the extrinsic coordinate system. $\left(x_S^E, y_S^E, z_S^E\right)$ are the coordinates of the centre of the laser scanner expressed in the extrinsic system and $\left(x_i, y_i, z_i\right)$, $i = 1, \ldots, n$ are the coordinates of the ith scanned point expressed in the intrinsic coordinate system. $\mathbf{R}_1$, $\mathbf{R}_2$, $\mathbf{R}_3$ – the matrices for rotation around the x-, y- and z-axes respectively; (ω, ϕ, κ) – the rotation angles from the extrinsic coordinates to the scanner intrinsic coordinates about the x-, y- and z-axes. The process is also known as georeferencing.

If the scanner is equipped with a dual-axis compensator, then the instrument's z-axis is parallel with the extrinsic system's z-axis and thus the rotation angles ω, ϕ_j become to zero, i.e. $\mathbf{R}_1$, $\mathbf{R}_2$ in Eq (4) are identical (unit) matrixes.

4. The case study

4.1. Description of the bridge

The European route E20 is a West-East United Nations (UNECE) across-sea route covering some 1880 km spanning Northern Europe from the United Kingdom, Ireland, Denmark, Sweden, Estonia and finally to Russia's second largest city Saint Petersburg. In Estonia the European route E20 connects the capital Tallinn and the third largest city Narva, located the eastern point of Estonia, by the Russian Federation border.

The load test presented in this study was performed on a bridge No. 156 located at kilometre 66 from Tallinn. The bridge crosses the Loobu River. The bridge was built in 1953 from reinforced concrete using a typical project from the year 1947 (*Sbornik tipovykh proektov zhelezobetonnykh i kamennykh iskustvennykh sooruzheniy. Vypusk 6. Zhelezobetonnye balochno-konsol'nye proletnye stroeniya. Prolety L0 – 12, 16, 20, 25 i 30 m. Gabarit G-7. Nagruzka N-10 i N-60. 1947*). The total length of the two-lane bridge was 31.2 m and width 8.5 m. The bridge was made of concrete mark M140 which by calculation had compression strength of $f_{ck} = 15$ MPa. The main reinforcement steel was mark St.3 (yield stress $f_y = 210$ MPa) with a diameter of 38 mm. The cover of the main reinforcement was 30 mm (Fig. 2). The form of the bridge structure was beam-type with two cantilevers 6.9 + 17.4 + 6.9 m. The bridge was originally designed to correspond load models N-10 and NG-60. According to former Soviet Union bridge norms the load model N-10 consists of several consecutive two-axle trucks where one of them weights 13 t (127.5 kN) and others 10 t (98 kN). The load model NG-60 consists of one caterpillar vehicle with a total load of 60 t (589 kN). The daily traffic frequency of the bridge was around 2700 cars – the carrying capacity and width appeared to be insufficient for contemporary needs. The general condition of the bridge was unsatisfactory before the testing – the index of condition was 63% out of 100% calculated by the Pontis Bridge Management System. That meant the bridge needed an overhaul or replacement during the next five years. An extensive corrosion of the reinforcement steel bars of the main beams had caused cracking of the concrete covers for reinforcement. Due to long-term self-weight and increased traffic load the main beams had also vertical cracks (their widths reached up to 0.1 mm).

After the load test the bridge was demolished.

4.2. Preliminary calculations and expected results

For pre-calculations of internal forces to occur during the bridge test load, all safety factors were taken from the former Soviet Union bridge norms (SNiP 2.05.*03-84 Mosty i truby*):
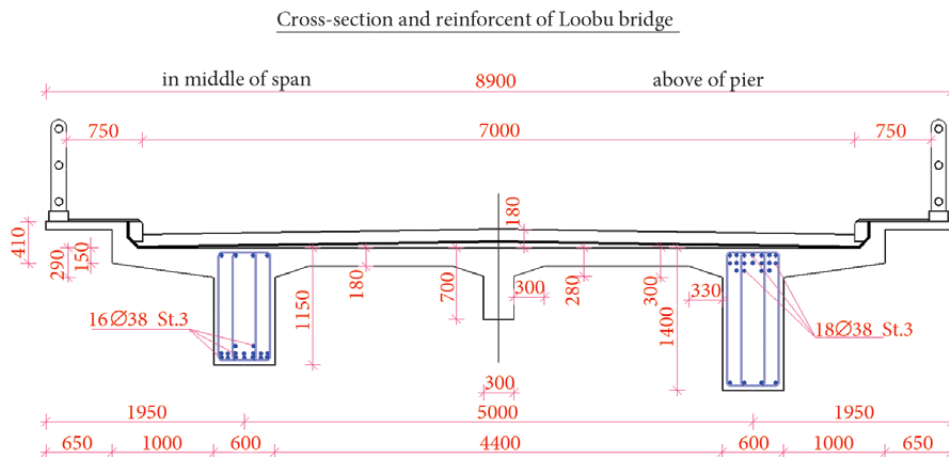

Fig. 2. A cross-section and reinforcement (depicted as blue dots and blue line in the beams) of the tested bridge

– for self-weight coefficient γ_f = 1.1;
– for N-10 γ_f = 1.4 and dynamic factor for 32.1 bridge length 1 + μ = 1.1;
– for NG-60 γ_f = 1.1.

Calculations were carried out using the 3D finite element program Bentley STAAD.Pro with different loading schemes (trucks, caterpillar vehicles, and other types of loads) Fig. 3.

The max bending moment (M_{Ed}) for the southern beam due to its own weight and the 60 t caterpillar vehicle was calculated to be 1916.5 kNm, yielding a predicted deflection of up to –13.6 mm. The calculated bending resistance (M_{Rd}) at the centre of the southern beam based on the material's strength properties given in the design project was 3387.0 kNm. The calculated bending resistance was almost twice the bending moment from the weight of the normative 589 kN (60 t) load. The max bending moment (M_{Ed}) from the designed test load of 1961 kN was calculated to be 5125.0 kNm, which is approx 1.5 times larger than the design bending resistance based on the bridge design project. The bending resistance (M_{Rd}), calculated by using material characteristic from the laboratory test was 5439 kNm, which was ~1.1 times larger than the bending moment from test load.

Based on preliminary calculations (Table 1) the designed test load is predicted to cause smaller bending moment (M_{Ed}) than the load capacity of the bridge.

The expected deflection from the max testing load was –50.3 mm (*EN 1992-1-1:2004 Eurocode 2: Design of Concrete Structures – Part 1-1*). However, using a linear-elastic calculation without cracking and Young's modulus obtained from laboratory testing of the concrete, the deflection was calculated to be –31.6 mm.

4.3. Design of the load test and visual deformation monitoring results

For the load test a hundred pieces of special two-ton metal blocks 2.00×0.40×0.35 m were used. The load test and the monitoring process were divided into four stages:
(i)   documenting the situation before the loading,
(ii) placement of the 785 kN load,
(iii) placement of the 823 kN load,
(iv) placement of the remaining 353 kN load.

The bridge was loaded in total with a total force of a load of 1961 kN (200 t), which clearly exceeds the designed load-bearing capacity of 589 kN (60 t), see section 4.1. The load (altogether 1961 kN) was piled up in the centre of the bridge on its southern side within 2×6 m rectangular area, Fig. 4. After the first two loading the bridge was set to sag for at least 30 min; after the loading of the remaining weights, the bridge was set to sag for at least 60 min. Monitoring begun after the deformations were stabilized.

In spite of fact that the total load exceeded the nominal carrying value more than three times, the bridge did not collapse. The main reasons to explain this was that the actual building materials used for the bridge components were much stronger than described in the original 1947 engineering project. The principles of calculation method for

reinforced concrete structures more than 60 ears ago were different compared to nowadays.

The laboratory tests results on the concrete specimen from the Loobu bridge proved that the compression strength of concrete (f_{ck} = 40 MPa) was approximately 2.7 times larger than in the design project (f_{ck} = 15 MPa). The high compression strength of concrete is partially explainable by the fact that compression strength increases in time. The average yield stress of the reinforcement (f_y = 295 MPa) was ~1.4 times higher than in the design yield stress f_y = 210 MPa. According to the former Soviet Union standard *GOST 380-57*, the steel mark St.3 has minimal characteristic yield strength of f_{yk} = 240 MPa and ultimate limit stress f_{uk} = 400−500 MPa. The laboratory test result of the tensile strength of reinforcement f_u was 426 MPa. The strength characteristics of the reinforcement steel used in the bridge construction meets the material class St.3.

Crack widths caused by the test loads at the bottom side of main beams reached up to 0.5 mm (in the middle of the span after every 15...20 cm), exceeding thus the allowed values of the serviceability limit state. The max admissible width of crack is 0.3 mm (*EN 1992-1-1:2004*).
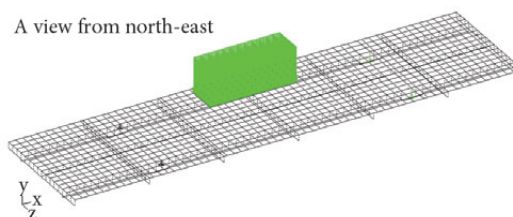

Fig. 3. Example of 3D model of the superstructure of the bridge with testing load

Fig. 4. Full load (1961 kN) placed on the bridge, image view from the scanners position from the Southern side of the bridge

Table 1. Bending moments and resistance's

	Bending resistance (M_{Rd})	Bending moment (M_{Ed})
Based on the bridge design project	3387 kNm	1916 kNm
Based on the load test design	5439 kNm	5125 kNm
Differences	62%	37%

4.4. Geodetic monitoring

The deformation monitoring of the load test was carried out using precise levelling and a novel terrestrial laser scanning technology. Precise levelling results were used to verify the accuracy of the TLS results in this study. Verifications of the TLS accuracy at bridge-works by modern electronic tacheometry is found, e.g. Mill *et al.* (2011). The monitoring process was carried out simultaneously but from different locations of the bridge; precise levelling on the deck of the bridge, whereas TLS observations were preceded from one side of the bridge aiming to observe the bottom surfaces of the cantilever beams.

4.4.1. Deformation monitoring using a precise levelling

A precise digital level Trimble DiNi03 with two calibrated invar bar code levelling staffs was used for determining bridge deformations. According to specifications the instrument's standard deviation is 0.3 mm on 1 km of double run levelling with invar precision bar code staffs. The precise levelling instrument Trimble DiNi03 and used invar bar code levelling staffs were calibrated and certified at the *Metrological Laboratory of the Finnish Geodetic Institute* in December 2010.

For deformation monitoring 20 reference points were embedded into the deck of the bridge (Fig. 5) at its northern and southern sides. A 0.60 m long steel rod as a temporary reference mark was embedded away from the bridge deck on a stabile soil. The levelling was accomplished from two stations placed away from the bridge deck.

The precise levelling was conducted before the loading and after each loading session.
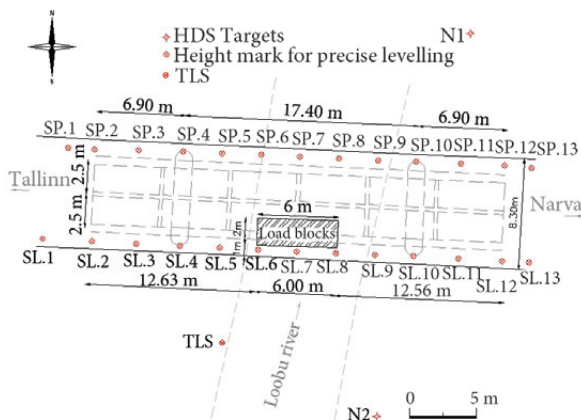

Fig. 5. Locations of the levelling height marks, TLS station, HDS targets and the load blocks. The bridge columns and cantilever beams with beam supports are exhibited by dashed lines
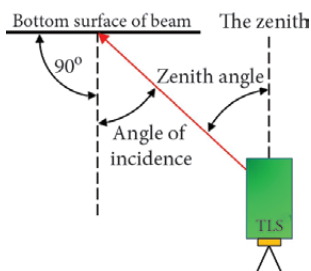

Fig. 6. Angle of incidence at scanning, the red line indicates the laser beam

4.4.2. Deformation monitoring using a TLS

A TOF Leica ScanStation C10 was used for monitoring of bridge deformations. The max range of the device is 300 m with a 360×270° field of view and max scanning rate of up to 50 000 points/sec. The manufacturer's accuracy specifications for the range and angle are ±4 mm and ±12 arc-sec, respectively. Several studies e.g. Abbas *et al.* (2013) and Antanavičiūtė *et al.* (2013) have investigated the calibration parameters of laser scanners Leica ScanStation C10. The results of the studies revealed only minor systematic errors in range measurement and in both horizontal and vertical angle measurement. The residuals corresponded with the manufacturer's accuracy specifications. Concerning the laser scanner Leica ScanStation C10 used in our study, it was calibrated before and after the bridge load test. In both occasions the same conclusion was reached and certified.

The TLS was erected at the best possible location at the distance of 6 m from the southern edge of the bridge (Fig. 5). It remained in the same location during the entire course of measuring. As the load test took place in early spring, when the ground had not yet thawed, the level compensator of the scanner was continuously monitored to detect and compensate any movements by the subsidence of the tripod.

Nevertheless, to ensure the scanning accuracy the scanner was reoriented before each TLS session using the 3″×3″ HDS (High-Definition Surveying) targets mounted near the bridge (Fig. 5). A detailed overview of TLS orientation methods therewith a registration method is given by Becerik-Gerber *et al.* (2011). Also Alba and Scaioni (2007) give a thorough overview of common registration processes and georeferencing techniques. The used TLS is equipped with a dual-axis compensator.

The scanner was set at the lowest location at the river bank to minimize incidence angles (Fig. 6) of laser beams. Recall, that placing the scanner under the bridge would have been hazardous due to the risk of the bridge collapsing. Lichti (2007) and Soudarissanane *et al.* (2007) suggest scanning at incidence angles below 65°, and moreover, Soudarissanane *et al.* (2011) states that increased incidence angles cause signal deterioration by approximately 20%. The actual incidence angle values at survey were between 80° and 87° at the southern and northern beams of the bridge, respectively. Although the incidence angle values were larger than the aforementioned threshold values, no remarkable unfavourable behaviour was detected from the achieved results.

Due to large incidence angles (80–87°), the angular precision determines the precision of the height of the scanned points. The law of error propagation is used to compute the precision of the height of the scanned point:

$$\sigma^2\left(\Delta\hat{h}\right) = \sum_{i=1}^{n}\left(\frac{\partial f}{\partial w_i}\right)^2 \sigma^2_{(w_i)}, \qquad (5)$$

where $\sigma^2\left(\Delta\hat{h}\right)$ denotes the combined variance of height increment with respect to the scanner origin. Note that $\Delta\hat{h}$ – an estimate (derived from the TLS range and angle

measurements, Eq (6)) of the actual height increment Δh; f – the function $\Delta h = f(w_i)$, $i = 1, ..., n$, relating the observations (w_i), $i = 1, ..., n$, and the height increment; $\sigma^2_{(w_i)}$ – the variance of the ith observable. The observation equation, i.e. function f, for the ith scanned point is written as:

$$\Delta\hat{h}_i = \rho_i \cos\varphi_i, \qquad (6)$$

where ρ_i – slope distance from the scanner to a contact point in the reflective surface; φ_i – zenith angle (Fig. 6); $\Delta\hat{h}$ – the resulting height increment.

Inserting Eq (6) into Eq (5) and calculating the derivatives, the combined standard uncertainty $\sigma(\Delta\hat{h})$ of the height increment of a survey point is found as:

$$\sigma(\Delta\hat{h}) = \pm\sqrt{\cos\varphi_i^2\sigma_{dist}^2 + \rho_i^2(-\sin\varphi_i)^2\sigma_{angle}^2}, \quad (7)$$

where σ_{dist} – the scanner's standard distance uncertainty; σ_{angle} – the scanner's standard angular uncertainty. Since $\sigma(\Delta\hat{h})$ depends on the angle φ_i, i.e. it is individual for each point i.

The combined standard uncertainties $\sigma(\Delta\hat{h})$ for the height increments at four points, two points on the southern beam and two points on the northern beam were calculated. The two points on the southern beam were located at distances (ρ) of 8.44 m and 19.66 m from the scanner at zenith angles (φ) of 81°02′ and 86°24′, respectively. The two points on the northern beam were located at distances of 13.43 m and 21.48 m from the scanner at zenith angles of 84°23′ and 86°53′, respectively. Numerical values for σ_{dist} and σ_{angle} were taken from the manufacturer's specifications.

Inserting these values into Eq (7) the mean value of four combined standard uncertainties of height increments $\sigma(\Delta\hat{h})$ of the survey points equals ±1.0 mm (one σ), which by adopting the 95% confidence interval (two σ) yields an uncertainty of ±2.0 mm. Thus the uncertainty of sequential TLS data sets (obtained from different monitoring epochs) equals to 2.0√2 = ±2.8 mm. Hence, the height differences exceeding ±2.8 mm between two TLS epochs at a location is considered as actual deformations.

5. Deformation analysis between different epochs

5.1. Results from TLS data

The processing of TLS data was conducted using a commercial 3D Point Cloud Processing Software Leica Cyclone developed by Leica Geosystems AG. The processing included removing noise from point clouds, creating surface meshes and deformation analysis between a surface created from the TLS data before the load test and surfaces created from TLS data from sequential load test epochs.

Under a load of 785 kN at its centre, the southern cantilever beam deflected by up to –1.8 cm (Fig. 7). Note that the western end of the beam rose by up to +0.6 cm; at the same time, the eastern end of the beam showed in some parts a deflection of up to –0.3 cm but no detectable rise.

A max deflection of –0.9 cm occurred at the centre of the northern cantilever beam (Fig. 7). The western end of the beam rose by up to +0.4 cm; at the same time, the eastern end of the beam showed in some places a deflection of up to –0.7 cm and in some cases a rise of up to +0.3 cm.

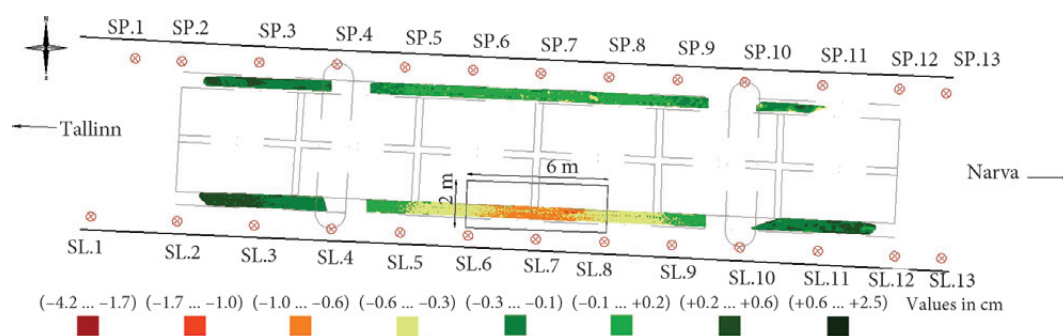Deformation measurement values derived from TLS data indicate that the centre southern cantilever beam,

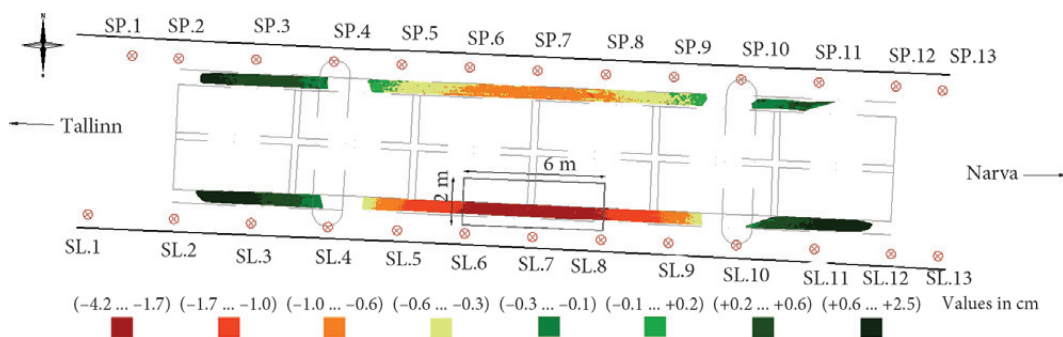**Fig. 7.** Results from the loading of 785 kN force

Fig. 8. Results from the loading of 1608 kN force

under a load of 1608 kN, deflected by a max of −3.0 cm (Fig. 8). Both the western and the eastern ends of the beam show a rise of up to +1.4 cm.

The centre northern cantilever beam deflected by up to −1.8 cm (Fig. 8). The western end of the beam shows a rise up of to +1.0 cm; the eastern end of the beam, a rise of up to +0.6 cm.

Deformation measurement values derived from TLS data when a max load of 1961 kN was applied indicate that the centre southern cantilever beam deflected by up to −4.2 cm (Fig. 9). The western end of the beam shows a rise up of to +2.2 cm; the eastern end of the beam, a rise up to +2.5 cm.

The centre northern cantilever beam showed a deflection of up to −2.4 cm (Fig. 9). The western end of the

beam showed a rise of up to +1.7 cm; the eastern end of the beam, a rise of up to +1.2 cm.

The deformation magnitudes agree roughly with the predictions (Section 4.2).

5.2. Comparison of precise levelling and TLS results

Precise levelling is based on difference of readings from a static invar bar code levelling staff positioned on a benchmark located some distance away from the bridge deck and readings from a second invar bar code levelling staff placed on embedded bolts to the bridge deck.

The bolts for levelling had to be placed a bit off from the exact location of the beams (Fig. 5). Therefore, in order to compare precise levelling results with TLS results, the longitudinal locations of the bolts were used as reference
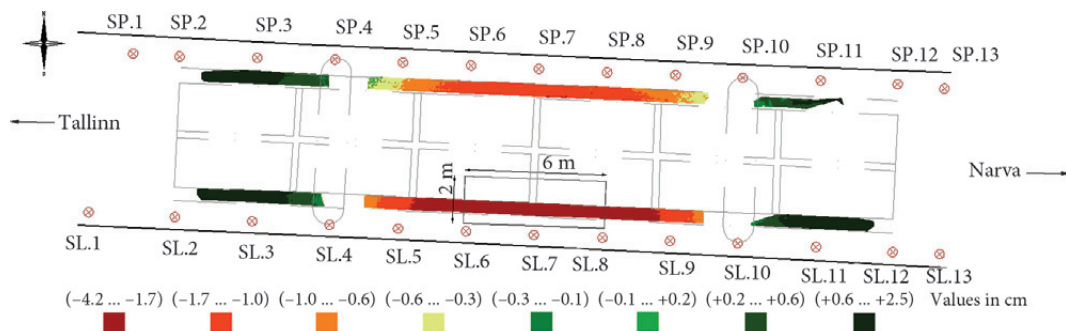

Fig. 9. Results from the loading of 1961 kN force

Table 2. Deformations determined by precise levelling and TLS

| Load, kN | Deformations detected by TLS, cm | | | | | | Deformations detected by precise levelling, cm | | | | | |
	Southern beam			Northern beam			Southern beam			Northern beam		
	Deflection	Rising		Deflection	Rising		Deflection	Rising		Deflection	Rising	
		West end	East end		West end	East end		West end	East end		West end	East end
758	−0.7	+0.3	+0.1	−0.3	+0.5	+0.2	−0.808	+0.428	+0.323	−0.123	+0.172	+0.051
1608	−2.1	+0.7	+0.6	−0.8	+1.0	+0.5	−2.269	+1.437	+1.282	−0.560	+0.784	+0.668
1961	−3.2	+1.2	+1.1	−1.4	+1.7	+1.0	−3.542	+2.394	+2.597	−1.111	+1.530	+1.686
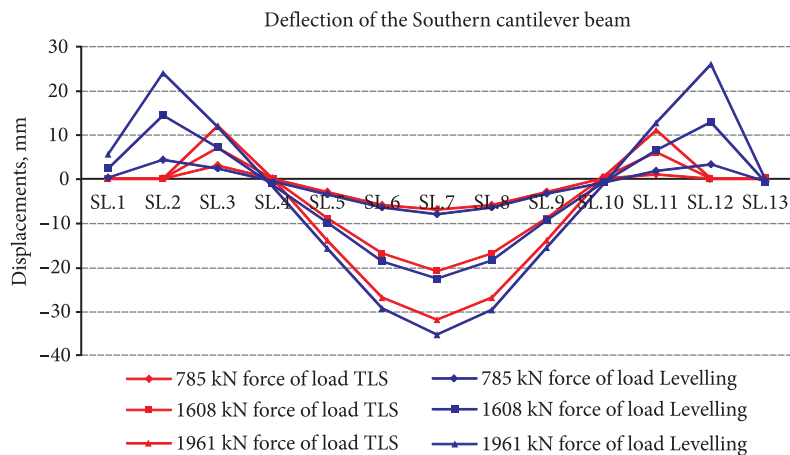
Fig. 10. Comparison of TLS and levelling results of the Southern beam. *Note:* at the centre of the beam (SL.7) deflection difference between TLS and levelling is under 785 kN + 0.108 cm; under 1608 kN + 0.169 cm; under 1961 kN +0.342 cm

points when determining the heights in the middle of the bottom surface of the beam, making the compared points equal in the longitudinal direction.

The TLS and levelling detected deformation values are presented and in Table 2.

Comparison of corresponding deformation values (Table 2) reveal a reasonable agreement between the TLS and precise levelling results. Note however, that TLS data is missing for the very beginning of the beams at SL 1–2 and SP 1–2; also TLS data is missing at the very end of the bridge deck at SL 12–13 and SP 12–13 (Figs 10 and 11) due to the limited bridge opening. From the comparison (Figs 10 and 11), a certain pattern for discrepancies emerges. The comparison results of the southern beam indicate that precise levelling results show slightly higher deflection values than TLS results; in the case of the northern beam, precise levelling results show slightly lower deflection values. Although the differences are noticeable, the differences are just within millimetres (detailed values are in Table 3).

The detected differences have occurred most likely due to the following. First, the accuracy of the TLS, since the TLS data uncertainty in this case was considered ±2.8 mm. Second, the TLS and precise levelling data were acquired from different surfaces – the TLS data addresses the bottom surface of beams, whereas the levelling was proceeded on the bridge deck. In addition, the differences were also due to the eccentric position of the load. When recalculating the precise levelling results by considering the inclination of the bridge due to the eccentric loading, the max displacement for the southern beam becomes –3.1 cm (TLS yielded –3.2 cm) and for the northern beam –1.5 cm (TLS –1.4), thus, the actual accuracy is estimated to be ±1 mm.

6. Conclusions

1. In this study a unique static load tests of a 60 year old cantilever beam bridge was presented. The loading test was divided into three loading and deformation monitoring stages. The stages consisted of forces of loads 785 kN, 1608 kN and with a max load of 1961 kN. The loading was carried out mainly on the southern cantilever beam but deformations were determined on the northern beam as well. For deformation monitoring terrestrial laser scanning technology simultaneously with precise levelling was applied. The pre-calculated max deflection of the bridge was –50.3 mm; according to precise levelling the actual deflection of the bridge deck at the max load of 1961 kN was –35.4 mm which is then 1.4 times smaller than pre-calculations predicted.

2. In spite of fact that the total load exceeded design value more than three times, the bridge did not collapse. The main reasons to explain this was that the actual materials were much stronger than described in engineering project and the principles of calculation method for reinforced concrete structures more than 60 years ago were different compared to nowadays. There were no significant
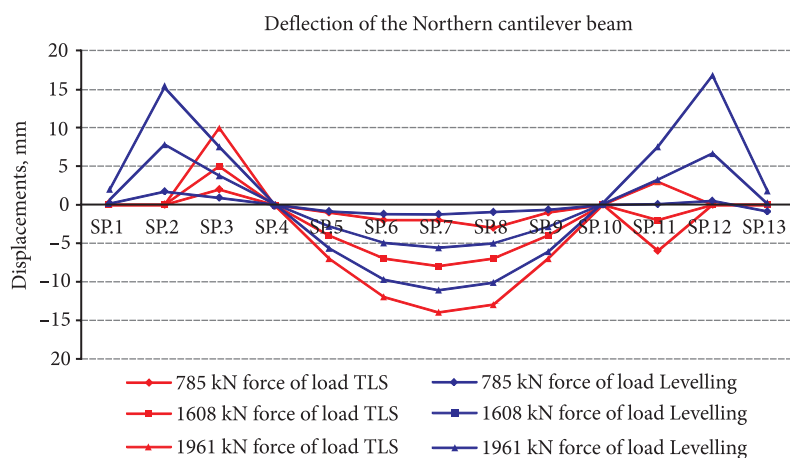

Fig. 11. Comparison of TLS and levelling results of the Northern beam. *Note:* at the centre of the beam (SP.7) deflection difference between TLS and levelling is under 785 kN –0.177 cm; under 1608 kN –0.24 cm; under 1961 kN –0.289 cm

Table 3. Comparison of deformation results

	Differences, cm					
	Southern beam			Northern beam		
Load, kN	Centre	West end	East end	Centre	West end	East end
758	+0.108	−0.128	−0.223	−0.177	+0.328	+0.149
1608	+0.169	−0.737	−0.682	−0.240	+0.216	−0.168
1961	+0.342	−1.397	−1.497	−0.289	+0.17	−0.686

Note: results are derived via TLS – Precise levelling, cf. Table 2.

damages of the bridge structure, only crack width exceeded the allowed values of the serviceability limit state almost two times. The study results are useful at further bridge load tests, since the novel technology provides unprecedented possibilities (as opposed to conventional surveying technologies) and excessive datasets for more extensive data analysis.

3. Results from this study confirm the assumed accuracy of terrestrial laser scanning on 95% confidence level of ±2.8 mm. The differences between terrestrial laser scanning and precise levelling vary within few millimetres. Therefore, in general TLS is suitable for detecting deformations within millimetre accuracy but it cannot be used for works demanding sub millimetre accuracy. However, terrestrial laser scanning allows acquiring high-resolution (almost continuous) data over the entire surface, in contrast to low-resolution point-wise levelling data. TLS technology allows remote monitoring of hazardous processes, thus, ensuring better safety of surveyors in such load tests. Note also that the terrestrial laser scanning data processing algorithms are currently still in the development phase. Within foreseeable future it will be possible to solve such complex data management tasks even more efficiently.

Acknowledgements

References

Abbas, M. A.; Setan, H.; Majid; Z.; Lichti, D. D.; Chong, K. A. 2013. A Self-Calibration of the Leica Scanstation C10 Scanner, in *Proc. of the IEEE Business Engineering and Industrial Applications Colloquium (BEIAC).* 7‒9 April 2013, Langkawi, Malaysia, 262‒266.
http://dx.doi.org/10.1109/BEIAC.2013.6560128

Alba, M.; Scaioni, M. 2007. Comparison of Techniques for Terrestrial Laser Scanner Data Georeferencing Applied to 3-D Modeling of Cultural Heritage, in *Proc. of the 3D-ARCH 2007 "Virtual Reconstruction and Visualization of Complex Architectures", XXXVI-5/W47.* 12–13 July 2007, Zurich, Switzerland.

Antanavičiūtė, U.; Obuchovski, R.; Paršeliūnas, E. K.; Popovas, M. G. D.; Šlikas, D. 2013. Some Issues Regarding the Calibration of the Terrestrial Laser Scanner Leica Scanstation C10, *Geodesy and Cartography* 39(3): 138–143.
http://dx.doi.org/10.3846/20296991.2013.840356

Becerik-Gerber, B.; Jazizadeh, F.; Kavulya, G.; Calis, G. 2011. Assessment of Target Types and Layouts in 3D Laserscanning for Registration Accuracy, *Automation in Construction* 20(5): 649–658. http://dx.doi.org/10.1016/j.autcon.2010.12.008

Bungey, J. H.; Millard, S. G. 1996. *Testing of Concrete in Structures.* Glasgow, United Kingdom: Chapman & Hall. 286 p. ISBN 0-203-48783-4.

Gruen, A.; Akca, D. 2005. Least Squares 3D Surface and Curve Matching, *ISPRS Journal of Photogrammetry and Remote Sensing* 59(3): 151–174.
http://dx.doi.org/10.1016/j.isprsjprs.2005.02.006

Lichti, D. D. 2007. Error Modelling, Calibration and Analysis of an AM–CW Terrestrial Laser Scanner System, *ISPRS Journal of Photogrammetry and Remote Sensing* 61(5): 307–324.
http://dx.doi.org/10.1016/j.isprsjprs.2006.10.004

Lichti, D. D. 2010. Terrestrial Laser Scanner Self-Calibration: Correlation Sources and Their Mitigation, *ISPRS Journal of Photogrammetry and Remote Sensing* 65(1): 93–102.
http://dx.doi.org/10.1016/j.isprsjprs.2009.09.002

Mill, T.; Ellmann, A.; Aavik, A.; Horemuz, M.; Sillamäe, S. 2014. Determining Ranges and Spatial Distribution of Road Frost Heave by Terrestrial Laser Scanning, *The Baltic Journal of Road and Bridge Engineering* 9(3): 227–236.
http://dx.doi.org/10.3846/bjrbe.2014.28

Mill, T.; Ellmann, A.; Uueküla, K.; Joala, V. 2011. Road Surface Surveying Using Terrestrial Laser Scanner and Total Station Technologies, in *Proc. of 8th International Conference Environmental Engineering.* Ed. by Čygas, D.; Froehner, K. D., 19–20 May 2011, Vilnius, Lithuania. Vilnius: Technika, 1142–1147.

Monserrat, O.; Crosetto, M. 2008. Deformation Measurement Using Terrestrial Laser Scanning Data and Least Squares 3D Surface Matching, *ISPRS Journal of Photogrammetry and Remote Sensing* 63(1): 142–158.
http://dx.doi.org/10.1016/j.isprsjprs.2007.07.008

Quintero, M. S.; Genechten, B. V.; de Bruyne, M.; Poelman, R.; Hankar, M.; Barnes, S.; Caner, H.; Budei, L., Heine, E.; Reiner, H.; García, J. L. L.; Taronger, J. M. B. 2008. *Theory and practice on Terrestrial Laser Scanning*. Training material based on practical applications. 241 p.

Reshetyuk, Y. 2009. *Self-Calibration and Direct Georeferencing in Terrestrial.* PhD thesis 978-91-85539-34-5. Stockholm: Kungliga Tekniska högskolan [Royal Institute of Technology]. Universitetsservice US AB.

Reshetyuk, Y. 2010. A Unified Approach to Self-Calibration of Terrestrial Laser Scanners, *ISPRS Journal of Photogrammetry and Remote Sensing* 65(5): 445–456.
http://dx.doi.org/10.1016/j.isprsjprs.2010.05.005

Riveiroa, B.; González-Jorgeb, H.; Varelab, M.; Jaureguic, D. 2013. Validation of Terrestrial Laser Scanning and Photogrammetry Techniques for the Measurement of Vertical Underclearance and Beam Geometry in Structural Inspection of Bridges, *Measurement* 46(1): 784–794.
http://dx.doi.org/10.1016/j.measurement.2012.09.018

Ryall, M. J. 2001. *Bridge Management.* Butterworth-Heinemann. 464 p. ISBN 978-0750650779.

Schulz, T. 2007. *Calibration of a Terrestrial Laser Scanner for Engineering Geodesy.* PhD thesis 17036. Berlin: Technical University of Berlin.

Soudarissanane, S.; Lindenbergh, R.; Menenti, M.; Teunissen, P. 2011. Scanning Geometry: Influencing Factor on the Quality

of Terrestrial Laser Scanning Points, *ISPRS Journal of Photogrammetry and Remote Sensing* 66(4): 389–399.
http://dx.doi.org/10.1016/j.isprsjprs.2011.01.005

Soudarissanane, S.; van Ree, J.; Bucksch, A.; Lindenbergh, R. 2007. Error Budget of Terrestrial Laser Scanning: Infuence of the Incidence Angle on the Scan Quality, in *Proc. of the 3D-NordOst 2007*. 6–7 September 2007. Berlin, Germany.

Staiger, R. 2003. Terrestrial Laser Scanning, Technology, Systems and Applications, in *Proc. of the 2ⁿᵈ FIG Regional Conference.* 2–5 December 2003, Marrakech, Morocco.

Tsakiri, M. L.; Pfeifer, N. 2006. Terrestrial Laser Scanning for Deformation Monitoring, in *Proc. of the 12ᵗʰ FIG symposium on Deformation Measurement and 3ʳᵈ IAG Symposium on Geod-esy for Geotechnical and Structural Engineering.* 22–24 May 2006, Baden, Austria.

Vosselman, G.; Maas, H.-G. 2009. *Airborne and Terrestrial Laser Scanning.* Dunbeath: Whittles Publisher. 320 p. ISBN 978-1439827987.

Zogg, H.-M.; Ingensand, H. 2008. Terrestrial Laser Scanning for Deformation Monitoring – Load Tests on the Felsenau Viaduct (CH), in *Proc. of the XXIst ISPRS Congress.* 3–11 July 2008, Beijing, China.